JOURNAL OF MORPHOLOGY 272:191–203 (2011)

A Unique Skeletal Microstructure of the Deep-Sea Micrabaciid Scleractinian Corals

Katarzyna Janiszewska,[1] Jarosław Stolarski,[1]* Karim Benzerara,[2] Anders Meibom,[3] Maciej Mazur,[4] Marcelo V. Kitahara,[5] and Stephen D. Cairns[6]

[1]*Institute of Paleobiology, Twarda, 00-818 Warsaw, Poland*
[2]*Institut de Minéralogie et de Physique des Milieux Condensés, UMR 7590, CNRS and IPGP Universités Paris 6 and 7. 140, rue de Lourmel, Paris 75015, France*
[3]*Muséum National d'Histoire Naturelle, Laboratoire de Minéralogie et Cosmochimie du Muséum (LMCM), UMR 7202, Case Postale 52, 61, rue Buffon, Paris 75005, France*
[4]*Department of Chemistry, Laboratory of Electrochemistry, University of Warsaw, Warsaw 02-093, Poland*
[5]*ARC Centre of Excellence in Coral Reefs Studies and Coral Genomics Group, James Cook University (JCU), Townsville, Queensland, Australia*
[6]*Department of Invertebrate Zoology, National Museum of Natural History, Smithsonian Institution, Washington, District of Columbia, Washington, D.C. 20560*

ABSTRACT Micrabaciids are solitary, exclusively azooxanthellate deep-sea corals belonging to one of the deepest-living (up to 5,000 m) scleractinian representatives. All modern micrabaciid taxa (genera: *Letepsammia*, *Rhombopsammia*, *Stephanophyllia*, *Leptopenus*) have a porous and often very fragile skeleton consisting of two main microstructural components known also from other scleractinians: rapid accretion deposits and thickening deposits. However, at the microstructural level, the skeletal organization of the micrabaciids is distinctly different from that of other scleractinians. Rapid accretion deposits consist of alternations of superimposed "microcrystalline" (micrometer-sized aggregates of nodular nanodomains) and fibrous zones. In contrast to all shallow-water and sympatric deep-water corals so far described, the thickening deposits of micrabaciids are composed of irregular meshwork of short (1–2 μm) and extremely thin (ca. 100–300 nm) fibers organized into small, chip-like bundles (ca. 1–2 μm thick). Longer axes of fiber bundles are usually subparallel to the skeletal surfaces and oriented variably in this plane. The unique microstructural organization of the micrabaciid skeleton is consistent with their monophyletic status based on macromorphological and molecular data, and points to a diversity of organic matrix-mediated biomineralization strategies in Scleractinia. J. Morphol. 272:191–203, 2011.

KEY WORDS: azooxanthellate scleractinian corals; biomineralization; microstructure; nanostructure

INTRODUCTION

The Micrabaciidae is a small scleractinian family present in the geologic record since the Early Cretaceous (~135 million years ago) and still existing today in the deep ocean. In morphological classifications, micrabaciids were grouped in the traditional suborder Fungiina (see Stolarski and Roniewicz, 2001), although Chevalier and Beauvais (1987: 695) suggested their association with Dendrophylliina, based on the "Pourtalès" pattern of septal arrangement and occurrence of the synapticular wall. Modern micrabaciids are attributed to four genera *Stephanophyllia* (Michelin, 1841), *Leptopenus* (Moseley, 1881), *Letepsammia* (Yabe and Eguchi, 1932), and *Rhombopsammia* (Owens, 1986), and the only fossil genus is *Micrabacia* (Milne Edwards and Haime, 1849). All recent micrabaciids are exclusively azooxanthellate (Cairns and Zibrowius, 1997) and (including *Micrabacia*) solitary in growth form, with the largest specimens reaching approximately 50 mm in calicular diameter.

Thirteen living species of micrabaciids are known from all ocean basins, including off continental Antarctica, occurring at depths of 49 to 5,000 m (see Cairns, unpublished data, http://www.lophelia.org/

Additional Supporting Information may be found in online version of this article.

Contract grant sponsor: Polish Ministry of Science and Higher Education; Contract grant number: project N307-015733; Contract grant sponsor: Muséum d'Histoire Naturelle in Paris; Contract grant sponsor: European Research Council Advanced Grant; Contract grant number: 246749 (BIOCARB); Contract grant sponsor: Region Ile-de-France; Contract grant number: SESAME 2000 E 1435 (JEOL JEM-2100F); Contract grant sponsors: INSU-CNRS, INP-CNRS and University Pierre et Marie Curie–Paris 6.

*Correspondence to: Jarosław Stolarski, Institute of Paleobiology, Twarda 51/55, 00-818 Warsaw, Poland. E-mail: stolacy@twarda.pan.pl

Received 18 June 2010; Revised 25 July 2010; Accepted 25 August 2010

Published online 15 November 2010 in Wiley Online Library (wileyonlinelibrary.com)
DOI: 10.1002/jmor.10906

pdf/Cold-water_Corals_Online_Appendix_000.pdf.). Modern micrabaciids have a light, lace-like skeleton with perforated wall and septa, and their polyps (edge-zone) completely cover the corallum. A combination of three main macromorphological characters is used to distinguish the Micrabaciidae: i) unique bifurcation patterns of septa and costae; ii) alternation of septal and costal insertions; and iii) presence of a calicular marginal shelf (Wells, 1933; Cairns, 1989). Recently, Kitahara et al. (2010) showed that micrabaciids form a deeply-diverging clade and represent the oldest phylogenetically scleractinian group with extant representatives based on mitochondrial gene *COI*. That finding encouraged us to select representatives of this group for more in-depth analysis of the skeleton with the prospect of finding microstructural criteria supporting monophyletic status of the group.

The conceptual link between skeletal microstructural characteristics and molecular phylogenetic reconstructions is based on the organic matrix-mediated biomineralization model (Lowenstam and Weiner, 1989). In this model, organic matrices composed of complex assemblages of macromolecules (proteins and polysaccharides) may control nucleation, spatial delineation, and organization of basic microstructural units. Initial attempts to use these refined, fine-scale morphological characters combined with skeletal-molecular studies have already shown their potential to provide support for molecular-based clades (Cuif et al., 2003b; Benzoni et al., 2007; Budd and Stolarski, 2009, 2010). These works showed clearly that traditional microstructural concepts such as "trabeculae" and "centers of calcification" (COC) (Bourne, 1887; Ogilvie, 1897; Vaughan and Wells, 1943) do not capture the full range of observed variation at the microstructural level. In particular, the complex relationships between the mineral and organic-enriched skeletal phases, and the spatial/temporal relationships between structurally different skeletal regions, cannot be described with these traditional concepts (see Cuif et al., 1998; Cuif and Dauphin, 2005b; Stolarski, 2003; Nothdurft and Webb, 2007; Brahmi et al., 2010). In recent work, the COC have been redescribed and reinterpreted as "rapid accretion deposits" (RAD) that are arranged in different ways and surrounded to varying degrees by "thickening deposits" (TD) (Stolarski, 2003; Brahmi et al., 2010). Briefly recapitulating, RAD are skeletal deposits formed within well-differentiated regions of skeletal rapid accretion, enriched in organic components. They can form a more or less continuous zone (cf. rapid accretion front of Stolarski, 2003) or can be separated from each other (cf. centers of rapid accretion of Stolarski, 2003). Thickening deposits are skeletal structures deposited outside the areas of rapid accretion and typically consist of layers of fibers continuous with those of RAD (not in acroporiids and, herein, described micrabciids; Nothdurft and Webb, 2007) but poorer in organic components.

The only attempt to investigate microstructural features of Micrabaciidae was carried out by Owens (1984) who followed traditional microstructural terminology and described micrabaciid septa as "composed of trabeculae—stacks of scleroderm-ites, which form the centers of calcification, arranged in a fan-like series radiating from a point near the base of the columella" (Owens, 1984: 520). Our literature-based observations (e.g., Owens, 1984: Fig. 5) suggested, however, that skeletal microstructure of micrabaciids is different from other Scleractinia, because well-defined crystal boundaries could not be identified within the fibrous skeleton. In this article, we provide a description of the unique microstructural organization of the skeleton in all genera of modern micrabaciids, which is a new apomorphy of this scleractinian clade.

MATERIAL AND METHODS

Material

Material used in this study consists of extant micrabaciid corals and azooxanthellate taxa collected by American, French, and Australian expeditions. All taxonomic details are given in figure captions, whereas locality data are provided in Supporting Information Appendix 1. Specimens illustrated in this article were subjected to various destructive analyses and the resulting thin sections, skeletal fragments attached to microscope stubs are housed at the Institute of Paleobiology, Polish Academy of Sciences, Warsaw (ZPAL).

Methods

Dry skeletons of micrabaciids were selected from museum collections or were extracted from formaldehyde or ethanol preserved specimens by removing the soft tissue by overnight immersion in 3% sodium hypochlorite (NaOCl) solution. The extracted coralla of all micrabaciid taxa (Supporting Information Appendix 1) were studied with transmitted light microscope (TLM), scanning electron microscope (SEM), and field emission scanning electron microscope (FESEM). Samples of *S. complicata* were studied with transmission electron microscope (TEM), samples of *L. discus* and *L. formosissima* were studied with atomic force microscope (AFM), and scanning X-ray microscope (SXM).

Thin (ca. 30-μm thick) and ultrathin (2- to 12-μm thick) sections of various skeletal elements were observed and photographed with a Nikon Eclipse 80i TLM. Skeletal microarchitectural and microstructural features were visualized with Philips XL 20 SEM and LEO1530 FESEM microscopes. Specimens were observed intact (septal surfaces), as broken but not etched skeletal samples, or as broken/polished and etched samples. Transverse or longitudinal polished or broken sections of septa were exposed for ~5 min etching in Mutvei's solution, following described procedures (Schöne et al., 2005). Similar effects were also obtained by ~20 s etching in 0.1% formic acid solution, following Stolarski (2003). The etched samples were rinsed with distilled water and air dried. Once dried, the samples were mounted on stubs with double-sided adhesive tape and sputter coated with conductive platinum film.

Atomic force microscopy was performed with a MultiMode Nanoscope IIIa (Digital Instruments, Veeco) following Stolarski and Mazur (2005). Standard silicone cantilevers were used for

measurements in tapping mode. Three signals (height, amplitude error, and phase) were simultaneously collected during each scan. The coral samples (septa cut transversely to their growth direction) were polished with diamond suspension of grain sizes 5 and 1 μm, and then with aluminum oxide (Buehler TOPOL 3 final polishing suspension with particle size 0.25 μm). After polishing, the sections were rinsed in Milli-Q water and washed in an ultrasonic cleaner for 10 s. The polished samples were then etched in 1% ammonium persulfate in McIlvain buffer (pH = 8) for 10 min, followed by rinsing in deionized water and drying.

Diffraction patterns of the skeleton's aragonite crystals were analyzed using a JEOL 2100F TEM operating at 200 kV, equipped with a field emission gun, a high-resolution UHR pole piece and a US4000 GATAN camera. Samples (ultrathin foils), cut from the middle of the septa, were prepared using a FEI STRATA DB 235 FIB (focused ion beam) milling machine equipped with a Ga liquid metal ion source (30-kV Ga beam after in situ deposition of a 1-μm-thick platinum layer). A ~20 × 5.5 × 1 μm^3 foil was transferred to a special omniprobe half-TEM grid within the vacuum chamber with an Omniprobe micromanipulator. This foil was subsequently further thinned to ~100 nm with decreasing ion-beam currents and at lower energy. Selected area electron diffraction (SAED) patterns were acquired using an aperture of 150 nm in diameter. For that purpose, orientation of the FIB foil was set so that one crystal was observed parallel to the [−112] zone axis. Then, keeping the FIB foil orientation fixed, the diffraction patterns of different areas showing high- and low-diffraction contrasts were checked. Electron diffraction patterns were recorded on a US4000 GATAN camera.

High-spatial resolution X-ray fluorescence mappings of sulfur content were performed at the X-ray microscopy beamline ID21 of European Synchrotron Radiation Facility, Grenoble, France, following Cuif et al. (2003a) procedures. The X-ray beam, monochromatized by means of double-crystal [Si(111)] fixed exit monochromator, was tuned to an energy just above the K-edge of sulfur. The Kirkpatrick-Baez mirror arrangement was used to focus the X-ray beam down to size of 0.3 × 0.8 μm^2. The X-ray fluorescence spectra were recorded by HpGe detector placed at 90° scattering angle. A 2D image was obtained by point-by-point scan of the sample across the focal point of the beam, with typical exposure time of 150–300 ms per point.

RESULTS

Four extant micrabaciid genera (*Leptopenus*, *Letepsammia*, *Rhombopsammia*, and *Stephanophyllia*) are clearly identified based on macromorphological characters (Cairns, 1989). However, at the microstructural level, all representatives of the group share very similar features. Figures 1–8, Table 1, and Supporting Information summarize our observations. References to particular taxa are made to highlight some structural differences or to indicate that only those species were examined.

Transmitted Light Microscopy Observations

Two main components are typically recognized in the skeleton of the examined micrabaciids (Figs. 1I, 4B, 5B,C, and Supporting Information Figs. 1, 2): rapid accretion deposits (RAD) and thickening deposits (TD).

In longitudinal sections of septa, RAD are composed of alternations of darker and brighter components (Figs. 4B, 5C, and Supporting Information Figs. 1A,D, 2B, see also Fig. 8). Darker components show microcrystalline structure, whereas lighter layers are formed by fibers (ca. 10–20 μm in length). The fibers show crystallographically ordered structure indicated by complete light extinction of fiber bundles every 90° during rotation of the section in polarized light (see transverse vs. longitudinal sections: Fig. 5B,C, respectively). In transverse thin-sections, RAD form a continuous mid-septal zone (up to 100-μm wide) or distinct regions that are separated from each other (cf. Stolarski, 2003). Depending on the vertical position of the transverse section, the central zone of sectioned RAD may consist of microcrystalline or fibrous deposits.

Thickening deposits are formed by short (ca. 1–2 μm) fibers whose variable orientation with respect to the section plane is illustrated by a wide range of interference colors (from black to maximum) and lack of coordinated light extinction within the groups of fibers. The boundaries between successive layers of TD are not sharp (Figs. 1I, 5B), although occasionally clear enough (alternation of more and less transparent layers) to observe their directions (Supporting Information Figs. 1D, 2E).

Longitudinal sections of the distal parts of septal teeth and spines show discontinuous RAD and TD regions: distal-most zones are composed of RAD only (Figs. 4B, 5B) and more proximal parts are formed by RAD surrounded by TD layers (Supporting Information Figs. 1E, 2A,B, F vs. Supporting Information Figs. 1D, 2E). Sectioned material often shows tiny fractures (Figs. 1I, 5C, 7) that, most commonly, are parallel to the skeletal surfaces (fractures follow direction of the growth layers).

SEM and FESEM Observations

At low/moderate magnifications (e.g., Fig. 2A,B), skeletal surfaces are relatively smooth, but septal faces of *Letepsammia*, *Stephanophyllia*, and *Rhombopsammia* are covered with pointed granules up to ~100-μm long. Occasionally, tips of septal spines/teeth are also covered with small (ca. 20 μm in diameter) and flat granules. At higher magnification (Figs. 1F, 5D), most of the skeletal surfaces are covered with flat, irregularly arranged, chip-like bundles of fibers, which usually are smaller than 1 μm in width and 1–2 μm in length. Chip-like microtexture is missing from the septal edges and other distal-most skeletal parts (tips of septal spines, etc.); those regions are either completely smooth or show linear grainy texture (e.g., Fig. 4D).

In etched sections of septa, the same microstructural components can be distinguished as under light microscopy: RAD and TD. Rapid accretion deposits form a homogenous mid-septal zone or are organized into centers of rapid accretion (CRA)

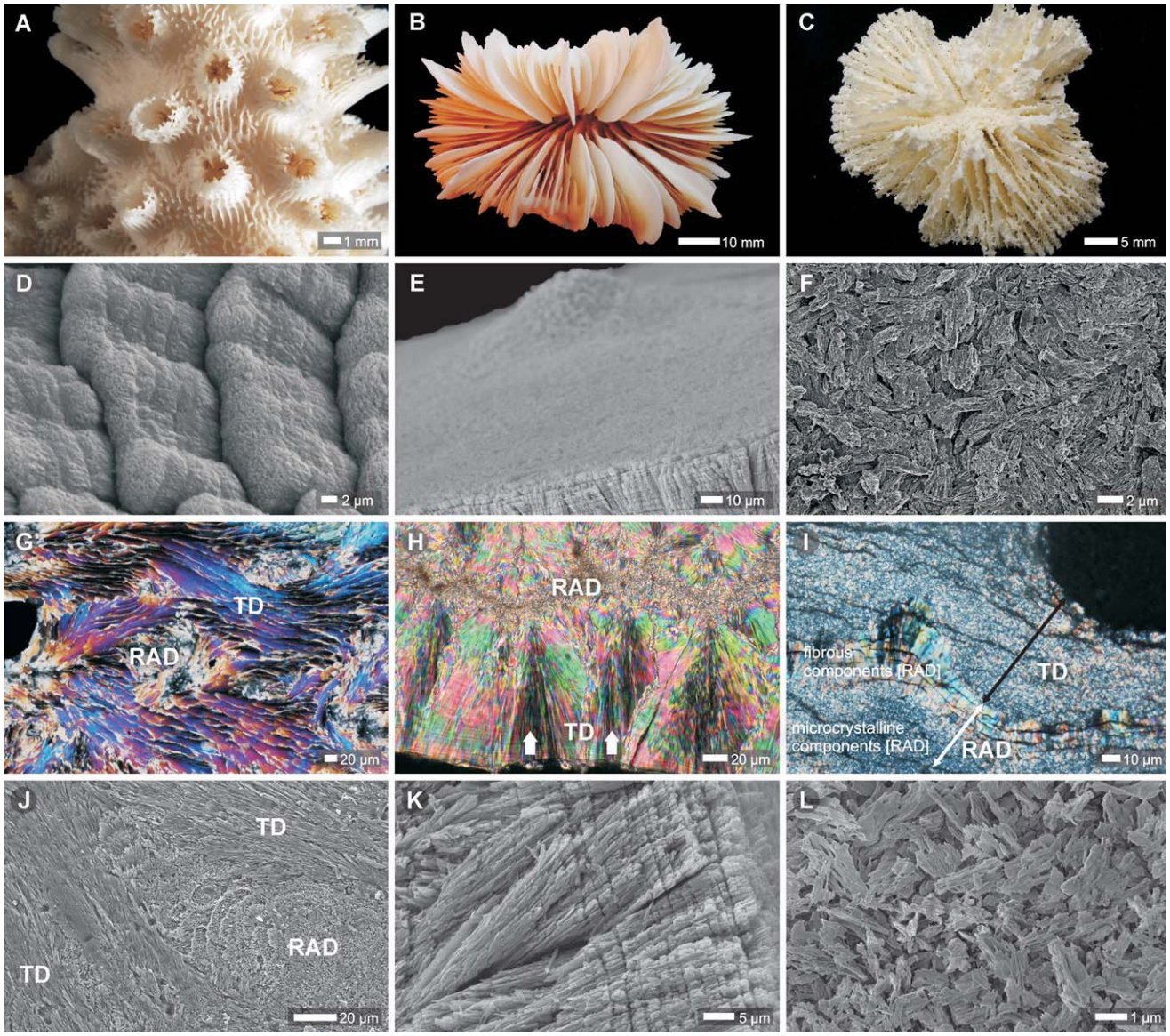

Fig. 1. Microscale skeletal characters of common zooxanthellate (*Acropora*, left column) and azooxanthellate (*Desmophyllum*, middle column) scleractinian taxa compared with similar features of typical micrabaciid *Rhombopsammia* (right column). **A**: Side view of the branch of *Acropora cervicornis* (Lamarck, 1816) [ZPAL H.25/12]; **B**: Distal view of *Desmophyllum dianthus* (Esper, 1794) [ZPAL H.25/5]; **C**: Distal view of Micrabaciid *Rhombopsammia niphada* Owens, 1986 [ZPAL H.25/11]; **D**: SEM micrograph of skeletal surface showing scale-like bundles of fibers of *Acropora cervicornis* (Lamarck, 1816) [ZPAL H.25/12]; **E**: SEM micrograph of smooth skeletal surface formed by densely packed tips of fiber bundles that are perpendicular to the septal surface of *Desmophyllum dianthus* (Esper, 1794) [ZPAL H.25/5]; **F**: SEM micrograph of septal surface covered with irregular meshwork of fiber bundles of Micrabaciid *Rhombopsammia niphada* Owens, 1986 [ZPAL H.25/11]. **G**: Transverse thin-section showing long, scale-like units of Thickening deposits (TD), subparallel to the septal plane of *Acropora cervicornis* (Lamarck, 1816) [ZPAL H.25/12]. Scale-like units, cut along their long axis, show uniform light extinction positions (polarized light), suggesting similar arrangement of crystallographic axes of fibers. **H**: Transverse sections of *Desmophyllum dianthus* (Esper, 1794) [ZPAL H.25/5] showing bundles of fibers (arrows) with complete light extinction (polarized light); **I**: Thin-section (polarized light) with "microcrystalline" (dark) and fibrous (vivid interference colors) RAD components of Micrabaciid *Rhombopsammia niphada* Owens, 1986 [ZPAL H.25/11]; crystallographically ordered structure of fibrous components is indicated by complete light extinction of fiber bundles every 90°. In contrast, short TD fibers show variable crystallographic orientation and lack of coordinated light extinction within the groups of fibers. Note fractures that follow direction of the growth layers; **J**: SEM micrograph (etched sample) of transverse thin-section showing long, scale-like units of Thickening deposits (TD), subparallel to the septal plane of *Acropora cervicornis* (Lamarck, 1816) [ZPAL H.25/12]; **K**: SEM micrograph (etched sample) of transverse sections of *Desmophyllum dianthus* (Esper, 1794) [ZPAL H.25/5] showing bundles of fibers (arrows) with complete light extinction; **L**: SEM micrograph (etched sample) of irregular meshwork of fibers on the transverse section of septumof Micrabaciid *Rhombopsammia niphada* Owens, 1986 [ZPAL H.25/11].

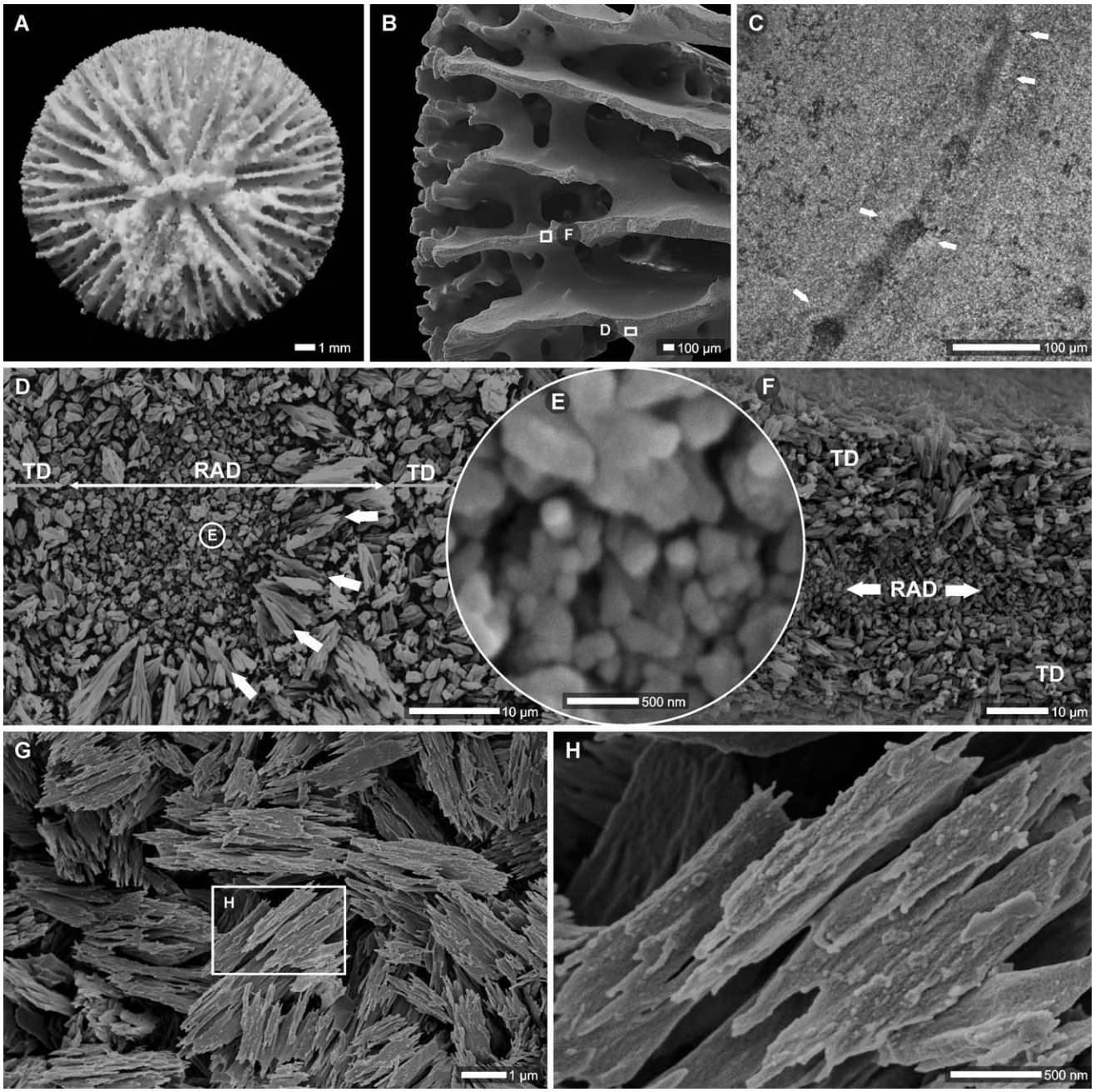

Fig. 2. Skeletal microstructure of micrabaciid *Stephanophyllia complicata* Moseley, 1876 [ZPAL H.25/10]. (**A**) Distal view of the entire corallum, and (**B**) broken, etched part of which various regions are magnified below; (**C**, polarized light) Thin-section with superimposed layers of "microcrystalline" (dark) vs. fibrous rapid accretion deposits (RAD) (arrows); thickening deposits (TD) are composed of short fibers with variable crystallographic orientation; (**D**) RAD often form continuous mid-septal zone (micrometer-size bundles of fibers (arrows) are part of RAD); (**E**) "Microcrystalline" RAD are aggregates of much smaller, nanocrystalline units. (**F**) RAD often form continuous mid-septal zone but can also be organized as CRA. (**G**) FESEM micrographs of TD composed of irregular meshwork of fibers organized into small bundles. (**H**) FESEM micrographs of close-up on the fiber bundles formed by extremely thin and short parallel fibers. (B, D–F) SEM.

composed of alternated "microcrystalline" and fibrous parts (Fig. 2D; see also Stolarski, 2003). The "microcrystalline" parts of RAD are aggregates of much smaller, nanocrystalline units (few tens of nanometers; Figs. 2E, 4F). Thickening deposits are composed of chip-like fiber bundles that show extremely thin (ca. 100–300 nm) and short (ca. 1–2 µm) parallel fibers (Figs. 2F,G, 4E, 5E,F). Bundles of fibers form an irregular meshwork within the skeleton but their longer axes are usually subparallel to the skeletal surfaces. Successive growth layers are not distinct.

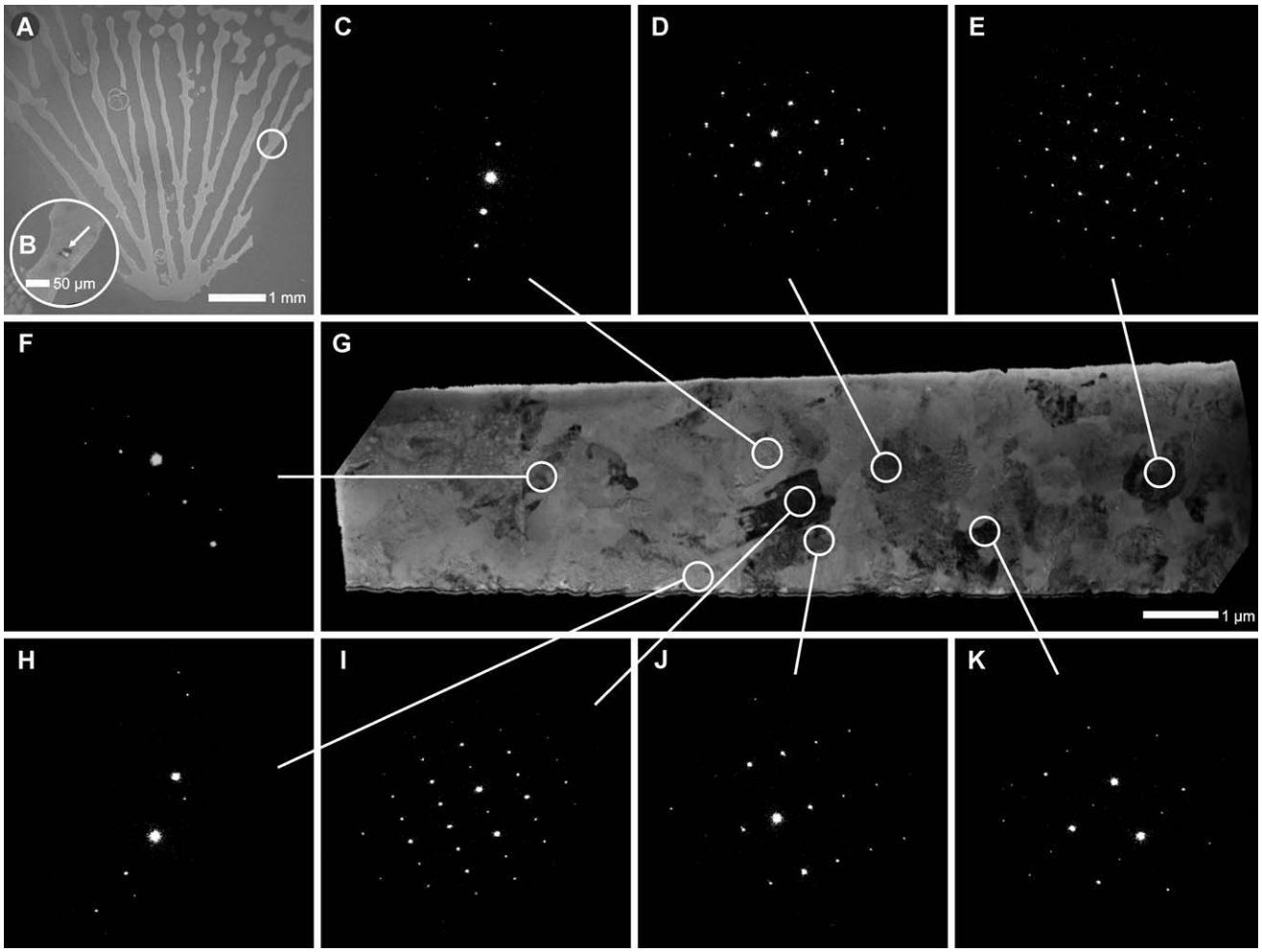

Fig. 3. TEM analysis of micrabaciid *Stephanophyllia complicata* Moseley, 1876 [ZPAL H.25/10]. (**A**) Transverse, thin-section with enlarged region showing localization of FIB foil (**B**). (**G**) Bright field image of the FIB foil. Electron diffraction patterns (C-F, H-K) were obtained from crystal regions marked on the FIB foil: determined zone axes for diffraction patterns (D), (E), (I), (J), and (K) are [121], [-112], [010], [-1-34] and [23-2] respectively.

AFM Observations

AFM observations of the polished and etched sections of *Letepsammia formosissima* (Fig. 6B,D,F) and *Leptopenus discus* (Fig. 6A,C,E) show that RAD regions have nanocomposite structure: mineral grains have ~30–100 nm in diameter and may form larger aggregates. Individual nanograins have a semicircular outline and are separated from each other by a few nanometers. As seen from the phase images, the material that separates or envelops individual nodular nanodomains is relatively soft (dark color on the image), which suggests that it is organic in nature (Fig. 6E,F).

TEM Observations

Using focused ion beam (FIB) milling, we prepared an ultrathin foil (<150 nm) from a septum of *Stephanophyllia complicata*. The selected region (section perpendicular to the septal plane) was composed of TD. Morphology of crystals observed in TEM is consistent with that shown by SEM (e.g., central crystal, SAED pattern i). Selected area electron diffraction patterns were all consistent with aragonite (Pnma, a = 5.744 Å, b = 4.96 Å, c = 7.97 Å). The sample was tilted so that one crystal (Fig. 3E) was observed parallel to the [−112] zone axis. Diffraction patterns of other randomly scattered areas showing weak and strong diffraction contrasts were checked subsequently. By indexing SAED patterns based on aragonite structure, it was observed that crystals do not show any particular common crystallographic arrangement.

SXM Observations

A map of sulfur distribution was made with the scanning X-ray microscope (SXM) operating in the X-ray fluorescence mode. Sulfur (probably associ-

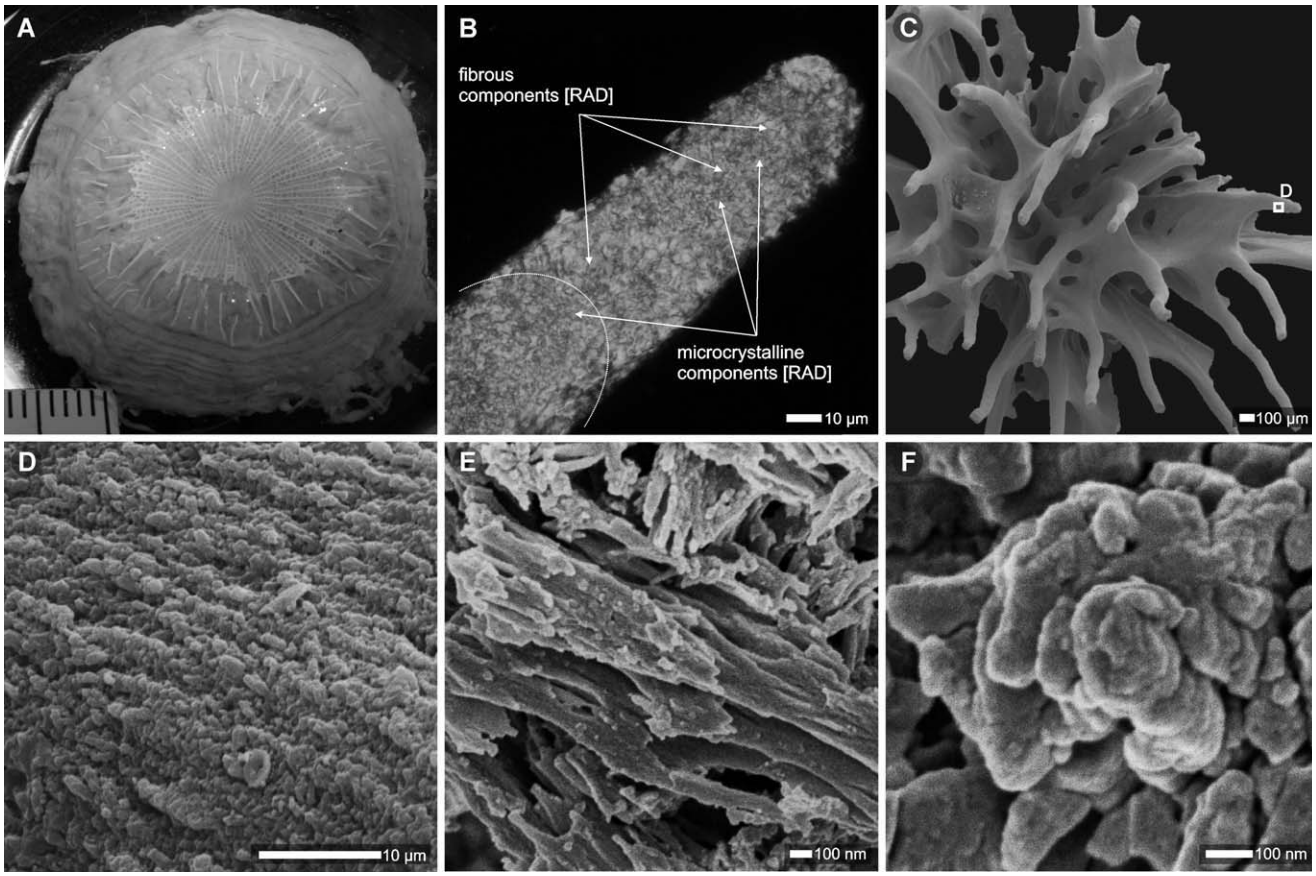

Fig. 4. Skeletal microstructure of micrabaciid *Leptopenus discus* Moseley, 1881 (ZPAL H.25/7). (**A**) Formaldehyde preserved specimen with the soft tissue (brown) constituting the main part of the animal; delicate skeleton (white) is deeply embedded within the polyp's tissue. (**B**) Longitudinal thin-section of septal spine with superimposed layers of "microcrystalline" vs. fibrous rapid accretion deposits (RAD). (**C**) Central part of the skeleton, and (**D**) close-up of the septal spine surface showing its linear texture. (**E**) Close-up of thickening deposits fibers. (**F**) Nanograins in rapid accretion deposits. (B) Polarized light, (C) SEM, and (D–F) FESEM micrographs.

ated with sulfated polysaccharides) shows a slight decrease in the central region of septum (Fig. 7C). Delicate banding corresponds to structural features visible in Fig. 7A,B. More transparent regions of the section (including fibrous zones) are slightly enriched in sulfur, whereas darker spots are depleted in sulfur.

DISCUSSION

The micrabaciids represent a unique biomineralization strategy among the scleractinian corals. The extant micrabaciids have been recovered from all oceans and from widely different depths (Supporting Information Appendix 1). Despite such a wide range of environmental conditions, a number of distinct skeletal properties, discussed below, are conserved among all representatives of this family. Furthermore, molecular data (Kitahara et al., 2010) show that the micrabaciids represent a phylogenetically well-defined clade. By comparison with other scleractinian coral clades that can be diagnosed based on microstructural criteria, our results strongly suggest that formation of the scleractinian skeleton is biologically controlled down to the microstructural level. It also suggests that this biological control is not easily perturbed by environmental factors, such as temperature, salinity, pressure, and probably also aragonite saturation state.

Structural and Compositional Aspects of the Micrabaciid Skeleton

At the macroscopic level, the fragile skeleton of micrabaciids is characterized by a unique bifurcation pattern of septa and costae, alternation of septal and costal insertions, and the presence of calicular marginal shelf (Cairns, 1989; see also Fig. 8).

At the microstructural level, the micrabaciid skeleton belongs to a rare category of scleractinian corals with RAD and TD spatially separated and

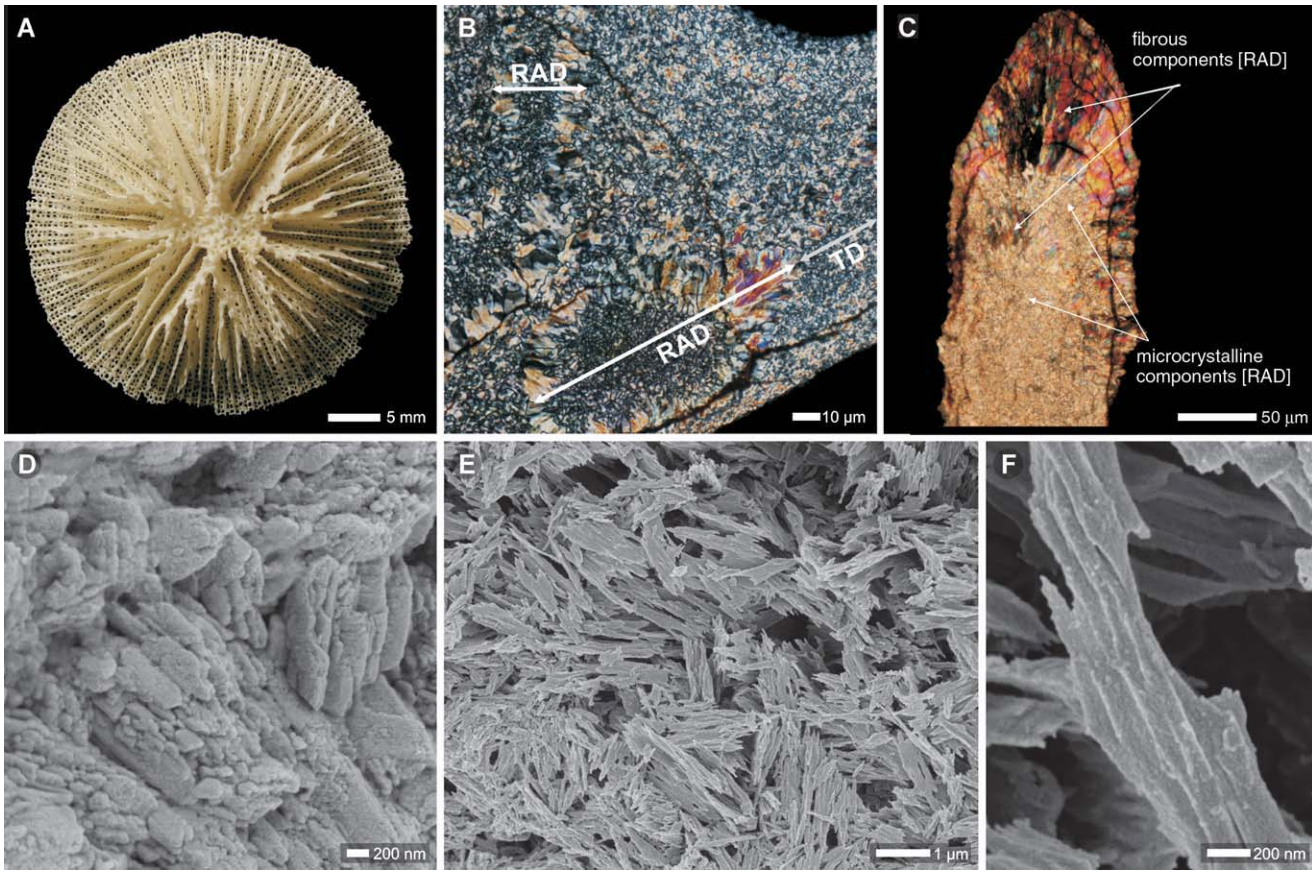

Fig. 5. Skeletal microstructure of micrabaciid *Letepsammia formosissima* (Moseley, 1876). (**A**) Distal view of the corallum. (**B**) Transverse thin-section of septum with rapid accretion deposits (RAD) with central "microcrystalline" zone surrounded by crystallographically aligned bundles of fibers; thickening deposits (TD) composed of short fibers with variable crystallographic orientation. (**C**) Longitudinal thin-section of septal lobe with superimposed layers of "microcrystalline" vs. crystallographically aligned bundles of RAD fibers (note lack of TD). (D–F) Irregular meshwork of fibers of TD on the skeletal surface (**D**). (**E**) TD-fibers in etched, transverse section of septum. Enlargement of a single bundle shows that it is formed by extremely thin, parallel fibers (**F**). (B,C) polarized light and (D–F) FESEM micrographs. A–C H.25/9; D–F H.25/8.

distinctly organized (Fig. 8; see different models of microstructural organization of the scleractinian skeleton in Stolarski, 2003; Cuif and Dauphin, 2005b; Nothdurft and Webb, 2007). The most distal parts of micrabaciid skeleton (teeth, septal lobes, or spines) are composed exclusively of RAD, that is, superimposed layers of organic-enriched "microcrystalline" and fibrous components (Figs. 4B, 5C; Supporting Information Fig. 2B,F). The surface of the RAD-composed skeletal parts is smooth and/or shows delicate longitudinal tracks of the fibers (e.g., Fig. 4D). In more proximal skeletal parts, TD become recognizable and are distinguishable from RAD regions by an irregular meshwork of fiber bundles (Supporting Information Fig. 1D).

Rapid accretion deposits. Microcrystalline RAD components in micrabaciid skeleton are formed by micrometer-sized aggregates of nodular nanodomains (typically 30–100 nm in diameter), which also have been reported in other scleractinian corals (Stolarski, 2003). However, in previous studies, the occurrence of nanodomains was usually not precisely correlated with the microstructural /mesostructural organization (see also Stolarski and Mazur, 2005; Cuif and Dauphin, 2005a,b). An interactive envelope, or cortex, that surrounds individual nodular nanodomains (Fig. 6D,F) is most likely formed by organic components and is particularly abundant in that zone (Stolarski, 2003; Cuif et al., 2005a,b). Nodular nanodomains have not been observed in other skeletal parts of micrabaciid skeleton (e.g., TD, fibrous RAD deposits) and this difference might be a result of different relative abundances of biopolymer between microcrystalline-RAD and fibrous-RAD/TD deposits. The importance of biopolymer composition on crystallization of nanocrystalline domains from the amorphous calcium carbonate precursors is suggested by biomimetic experiments (Meldrum and Cölfen, 2008).

In all examined micrabaciid coralla, the RAD are composed of superimposed organic-enriched

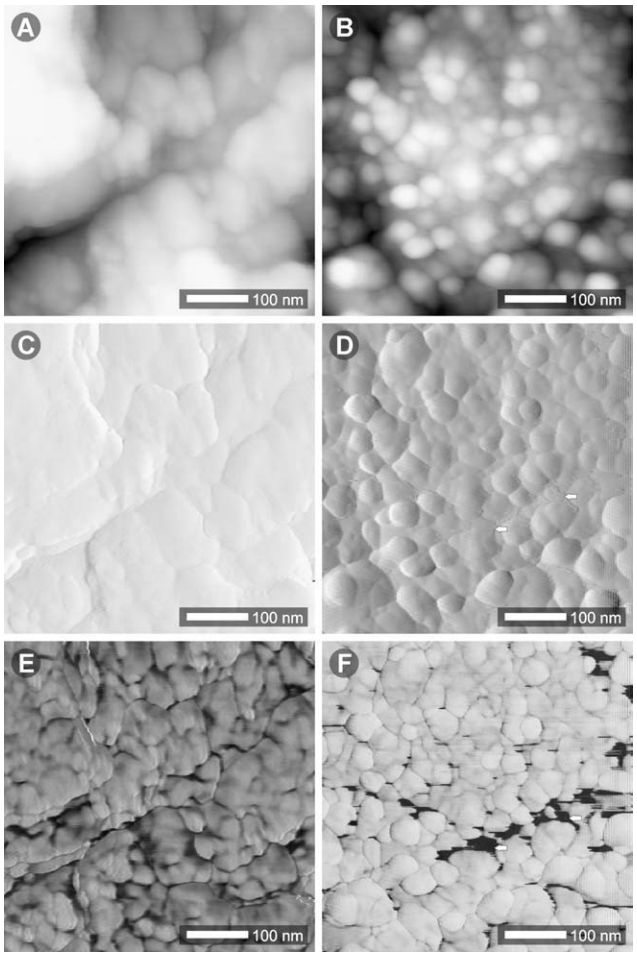

Fig. 6. AFM images showing nanocomposite structure of the rapid accretion deposits ("microcrystalline" regions) of micrabaciids (**A**, **C**, **E**) *Leptopenus discus* Moseley, 1881 [ZPAL H.25/7] and (**B**, **D**, **F**) *Letepsammia formosissima* (Moseley, 1876) [ZPAL H.25/9]. Individual nanodomains are enveloped by a material with a different interaction with the AFM tip—most likely organic materials (arrows in D, F). Height–2D projection (A, B), amplitude (C, D), and phase (E, F) images.

"microcrystalline" and fibrous layers. This is consistent with observations of longitudinally sectioned RAD in other scleractinians (Wise et al., 1970; Wise, 1972; Jell, 1974; Jell and Hill, 1974; Stolarski, 2003; Nothdurft et al., 2006) and suggests a common physiological mechanism responsible for this structural alternation, irrespective of ecological (shallow water vs. deep water) and physiological (zooxanthellate vs. azooxanthellate) conditions. Differences between RAD components among various taxonomic groups are related to i) their diameter (e.g., *Flabellum*, ca. 10 μm vs. *Platygyra*, ca. 20 μm; Stolarski, 2003), ii) isolated vs. continuous arrangement along the growing front of a septum (e.g., *Guynia* vs. *Truncatoguynia*; Stolarski, 2000), iii) formation of larger aggregations (e.g., in traditional Faviina, see Budd and Stolarski, 2009), and iv) the relative thickness of the microcrystalline vs. fibrous zones (e.g., thick TD zone in many traditional mussids vs. narrow TD zone in Fungiacyathidae, see Budd and Stolarski, 2009; Stolarski, unpublished data).

Thickening deposits. The main microstructural feature that distinguishes micrabaciids from all other scleractinian groups is the structure of their TD. Traditionally, thickening deposits (fibers) are considered as bundles of biocrystals oriented more or less perpendicularly to the growing surfaces. This is actually observed in many corals with relatively smooth skeletal surfaces (e.g., *Desmophyllum*, *Guynia*, see Stolarski, 2000, 2003). However, in corals with more complex skeletal surfaces textures, the microstructural organization is also more diversified (preliminary study by Stolarski, 2007). For example, vesicular or lens-shaped fibrous units outlined by organic envelopes occur in corals with microtuberculated or "gooseflesh" skeletal microtexture (e.g., *Seriatopora*, *Pocillopora, Gardineria*, *Anthemiphyllia*), whereas laminar microstructural organization of TD are observed in corals with scale-like (shingle) surface texture (e.g., *Acropora*, *Flabellum*). In micrabaciids, skeletal elements thickened by TD can be easily distinguished from RAD regions by their irregular crisscross pattern of bundles of fibers observed on the skeleton surface. This pattern reflects the internal organization of TD, which consists of chip-like bundles of extremely thin fibers. The chip-like bundles form an irregular meshwork within the skeleton: longer axes of fiber bundles are subparallel to the skeletal surfaces but show variable crystallographic orientation within this plane. One result of this variable orientation of TD fibers is a lack of distinct boundaries between successive growth layers.

Sulfated polysaccharides. Sulfated polysaccharides occur in calcareous skeletons of various organisms including corals (Cuif et al., 2008). Among scleractinian corals examined so far (i.e., *Favia stelligera*, *Lophelia pertusa*, see Cuif et al., 2003a; *Acropora digitifera*, *Diploastrea labyrinthica*, *Montastraea curta*, *Porites* cf. *australiensis*, see Cuif and Dauphin, 2005a), the RAD (or centers of calcification) have been found to be relatively S enriched if compared with the surrounding fibrous aragonite. However, in the septa of the micrabaciid *L. formosissima*, the sulfur distribution (Fig. 7C) is not similar to these previous data. Fluorescence observed at 2.4817 keV, corresponding to the main peak of S K-edge spectra of sulfated polysaccharides (chondroitin sulfate A; Cuif et al., 2003a) indicate that the RAD and TD contain about the same level of S. The lack of distinct S banding within *Letepsammia* TD is likely to be the result of the absence of clear boundaries between successive layers in the TD. Furthermore, the central part of septum of *L. formosissima* containing the RAD does not show rel-

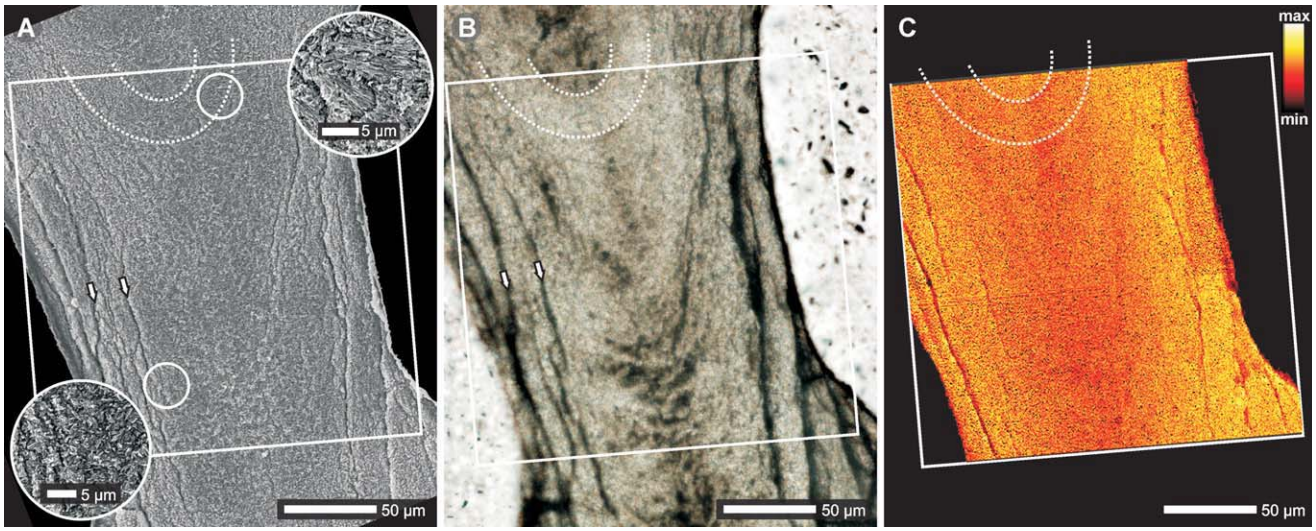

Fig. 7. Transversally sectioned septum of micrabaciid [ZPAL H.25/8] *Letepsammia formosissima* (Moseley, 1876) in SEM (**A**, etched surface) and transmitted light (**B**, thin section) views compared with scanning X-ray microscope 2D microfluorescence map of sulfur distribution (**C**). Encircled regions in (A) shows irregular meshwork of fiber bundles of the TD (lower-left circle) and fibers of RAD deposits (upper-right circle). Sulfur (probably associated with sulfated polysaccharides) shows slight decrease in the central region of septum; delicate banding corresponds to structural features visible in A,B. More transparent regions of the section (including fibrous zones) are slightly enriched in sulfur. Arrows (A,B) mark tiny fractures that follow direction of the growth layers.

ative S enrichment. This could indicate that, due to the unusual ultrastructural organization of the micrabaciid skeleton, the abundance of organic materials, including polysaccharides, is fairly homogeneous in the septa. However, additional analyzes are underway to test this hypothesis.

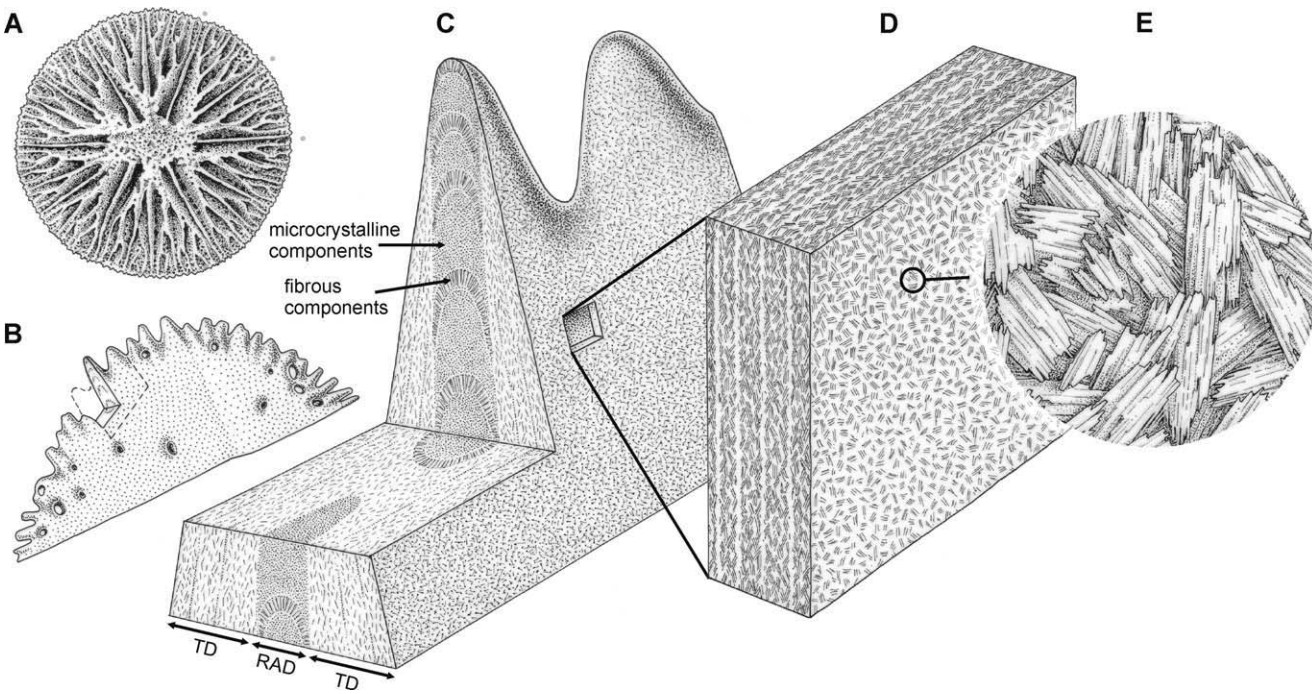

Fig. 8. Macrostructural and microstructural characters of micrabaciid skeleton. (**A**) Distal view of corallum with straight septa of two first cycles (grey dots in one sextant) and multiple bifurcations of other cycles. (**B**) Distal part of perforated septum with position of the portion enlarged in (**C**). Idealized, three-dimensional model of micrabaciid skeletal microstructure. Rapid accretion deposits (RAD) are composed of alternations of "microcrystalline" (micrometer-sized aggregates of nodular nanodomains) and fibrous zones. Distalmost parts of the skeleton are composed exclusively of RAD and more proximal parts are covered by layers of TD. TD consists of irregular meshwork of fiber bundles oriented subparallel to the surface (D,E).

TABLE 1. Summary of microstructural observations (references to illustrations)

	Micrabaciidae				Acroporidae	Caryophylliidae
Taxa	*Leptopenus discus* (Moseley, 1881)	*Letepsammia formosissima* (Moseley, 1876)	*Rhombopsammia niphada* (Owens, 1986)	*Stephanophyllia complicata* (Moseley, 1876)	*Acropora cervicornis* (Lamarck, 1816)	*Desmophyllum dianthus* (Esper, 1794)
TD: chip-like bundles that form an irregular meshwork within the skeleton	Figure 4E (section)	Figures 5D (surface), 5E (section), and 3 (TEM)	Figure 1F (surface), 1L (section)	Figure 2G,H (surface), F (section)	—	—
TD: other microstructural patterns	—	—	—	—	Fibers organized into scale-like (shingle) units subparallel to the growing surfaces (Fig. 1D,G,J)	Fibers oriented more or less perpendicularly to the growing surfaces (Fig. 1E,H,K)
RAD: darker (microcrystalline) and brighter (fibrous) components	Figure 4B (longitudinal section), Supporting Infomation Figure 2B (longitudinal section)	Figure 5C (longitudinal section), Supporting Information Figures 1D (longitudinal sections), 1E (transverse section), 7A,B (transverse section)	Figure 1I (transverse section)	Figure 2C (longitudinal, oblique section)	See longitudinal sections of *Acropora hyacinthus* (Nothdurft and Webb, 2006: Fig. 13A,C)	Stolarski, 2003: Figure 7F,G (longitudinal sections)
RAD: nanocomposite structure of "microcrystalline" regions	Figures 4F, 6A,C,E	Figure 6B,D,F	Not examined	Figure 2E	Nanocomposite structure of scleractinian skeleton is widely recognized (Cuif et al., 2005a,b; Stolarski and Mazur, 2005; Przenioslo et al., 2008), however, the occurrence of nanodomains was usually not precisely correlated with the microstructural/mesostructural organization. Nanocomposite structure of RAD in *Desmophyllum* and *Acropora* has been recognized but is a subject of separate publication.	

The main microstructural character that distinguishes micrabaciids from all other scleractinians (*Acropora* and *Desmophyllum* are given as examples) is the chip-like organization of their thickening deposits (TD). The structure of rapid accretion deposits (RAD) seems to be similar in Scleractinia.

Molecular Data and the Possible Link with the Skeletal Microstructures

Over the past few years, in-depth skeletal studies of various groups of Scleractinia were undertaken, showing remarkable diversity in organization of organomineral skeletal units. Preliminary attempts at using those fine-scale characters in combined skeletal-molecular studies have shown their potential to resolve conflicting results between molecular and traditional classifications (Cuif et al., 2003b; Benzoni et al., 2007; Budd and Stolarski, 2009, 2010). The diversity of skeletal microstructural patterns and their close association with members of some molecularly distinguished clades suggest a genetically coded biological control of mineralization (organomatrix-controlled skeletogenesis). Possible agents of such biomineralization control include organic macromolecules, in particularly proteins, whose functional significance in biomineralization has been tested in vitro in various groups of organisms (e.g., in mollusks, see Falini et al., 1996; Gotliv et al., 2003; Fu et al., 2005; Kim et al., 2006). Proteinaceous components intimately associated with the mineral phase have also been described in scleractinian skeletons (Fukuda et al., 2003; Puverel et al., 2005). Research on gene expression that encode such proteins (galaxins and amgalaxin-like molecules) suggested that both types of molecules are involved in the deposition of two structurally different mineral components. Galaxins may be involved in controlling the fiber-like aragonite, and Amgalaxin-like molecules are associated with granular calcification (Reyes-Bermudez et al., 2009). These studies herald a new type of combined molecular and structural analyses aiming at finding a link between hierarchical organization of skeletal biocrystals and functionality of organic macromolecules secreted by the coral organism that actively participate in the biomineralization processes. We expect that such a link may appear strong among corals showing a very distinct microstructural organization, and whose molecular phylogenetic position is well established. Up to now, the most striking example of this kind was acroporiids, which is the largest group of modern Scleractinia. This group forms a well-supported molecular clade (Wei et al., 2006), and all representatives show unique, scale-like organization of TD deposits (Wallace and Wolstenholme, 1998). The distinct and consistent microstructure of TD deposits in micrabaciids supports the monophyletic status of the group suggested by molecular phylogeny (Kitahara et al., 2010). Ongoing research is aimed at finding a common biochemical characteristic of micrabaciid organic molecules that may be responsible for unique microstructural organization of TD fibers.

ACKNOWLEDGMENTS

The authors thank the reviewers (Luke D. Nothdurft, Queensland University of Technology, Australia, and an anonymous reviewer) for their valuable comments. The authors thank David Troadec at IEMN (Villeneuve d'Ascq, France) for the preparation of FIB foils.

LITERATURE CITED

Bourne GC. 1887. On the anatomy of *Mussa* and *Euphyllia*, and the morphology of the madreporarian skeleton. Q J Microsc Sci London 41:499–547.

Benzoni F, Stefani F, Stolarski J, Pichon M, Mitta G, Galli P. 2007. Debating phylogenetic relationships of the scleractinian *Psammocora*: Molecular and morphological evidences. Contrib Zool 76:35–54.

Brahmi C, Meibom A, Smith DC, Stolarski J, Auzoux-Bordenave S, Nouet J, Doumenc D, Djediat C, Domart-Coulon I. 2010. Skeletal growth, ultrastructure and composition of the azooxanthellate scleractinian coral *Balanophyllia regia*. Coral Reefs 29:175–189.

Budd AF, Stolarski J. 2009. Searching for new morphological characters in the systematics of scleractinian reef corals: Comparison of septal teeth and granules between Atlantic and Pacific Mussidae. Acta Zool 90:142–165.

Budd AF, Stolarski J. 2010. Corallite wall and septal microstructure in scleractinian reef corals: Comparison of molecular clades within the family Faviidae. J Morphol (in press).

Cairns SD. 1989. A revision of the ahermatypic Scleractinia of the Philippine Islands and adjacent waters, Part 1: Fungiacyathidae, Micrabaciidae, Turbinoliinae, Guyniidae, and Flabellidae. Smithson Contrib Zool 486:1–136.

Cairns SD, Zibrowius H. 1997. *Cnidaria anthozoa*: azooxanthellate Scleractinia from the Philippine and Indonesian regions. Mém Mus Natl Hist Nat 172:27–243.

Chevalier J-P, Beauvais L. 1987. Ordre des Scléractiniaires. In: Grasse PP, editor. Traité de Zoologie, Cnidaires, Anthozoaires, Masson: Paris. pp 403–764.

Cuif J-P, Dauphin Y. 2005a. The environment recording unit in coral skeletons—a synthesis of structural and chemical evidences for a biochemically driven, stepping--growth process in fibers. Biogeosciences 2:61–73.

Cuif J-P, Dauphin Y. 2005b. The two-step mode of growth in the scleractinian coral skeletons from the micrometre to the overall scale. J Struct Biol 150:319–331.

Cuif J-P, Dauphin Y, Gautret P. 1998. Compositional diversity of soluble mineralizing matrices in some recent coral skeletons compared to fine-scale growth structures of fibers: Discussion of consequences for biomineralization and diagenesis. Int J Earth Sci 88:582–592.

Cuif J-P, Dauphin Y, Doucet J, Salome M, Susini J. 2003a. XANES mapping of organic sulfate in three scleractinian coral skeletons. Geochim Cosmochim Acta 67:75–83.

Cuif J-P, Lecointre G, Perrin C, Tillier A, Tillier S. 2003b. Patterns of septal biomineralization in Scleractinia compared with their 28S rRNA phylogeny: A dual approach for a new taxonomic framework. Zool Scr 32:459–473.

Cuif J-P, Dauphin Y, Farre B, Nehrke G, Nouet J, Salomé M. 2008. Distribution of sulphated polysaccharides within calcareous biominerals suggests a widely shared two-step crystallization process for the microstructural growth units. Mineral Mag 72:233–237; doi: 10.1180/minmag.2008.072.1.233.

Esper EJC. 1794. Fortsetzungen der Pflanzenthiere, Vol. 1. Raspe: Nürnberg. pp 1-64.

Falini G, Albeck S, Weiner S, Addadi L. 1996. Control of aragonite or calcite polymorphism by mollusk. Science 271: 67–69.

Fu G, Valiyaveettil S, Wopenka B, Morse DE. 2005. $CaCO_3$ biomineralization: Acidic 8-kDa proteins isolated from aragonitic abalone shell nacre can specifically modify calcite crystal morphology. Biomacromolecules 6:1289–1298.

Fukuda I, Ooki S, Fujita T, Murayama E, Nagasawa H, Isa Y, Watanabe T. 2003. Molecular cloning of a cDNA encoding a

soluble protein in the coral exoskeleton Biochem Biophys Res Commun 304:11–17.
Gotliv BA, Addadi L, Weiner S. 2003. Mollusk shell acidic proteins: In search of individual functions. Chembiochem 4:522–529.
Jell JS. 1974. The microstructure of some scleractinian corals. Proceedings of the 2nd International Coral Reef Symposium, Brisbane, Australia, 1973, 22nd June-2nd July, 2:301–320.
Jell JS, Hill D. 1974. The microstructure of corals. In: Sokolov BS, editor. Ancient Cnidaria, Vol. 1. Nauka: Novosibirsk. pp 8–14.
Kim IW, Collino S, Morse DE, Evans JS. 2006 A crystal modulating protein from molluscan nacre that limits the growth of calcite in vitro. Cryst Growth Des 6:1078–1082.
Kitahara MV, Cairns SD, Stolarski J, Blair D, Miller DJ. 2010. A comprehensive phylogenetic analysis of the Scleractinia (Cnidaria, Anthozoa) based on mitochondrial CO1 sequence data. PLoS ONE 5:e11490; doi:10.1371/journal.pone.0011490.
Lamarck JB. 1816. Histoire naturelle des Animaux sans vertébres 2. Les Polypes. Verdiére: Paris. pp 1–568.
Lowenstam HA, Weiner S. 1989. On Biomineralization. Oxford University Press: New York. pp 1–324.
Meldrum FC, Cölfen H. 2008. Controlling mineral morphologies and structures in biological and synthetic systems. Chem Rev 108:4332–4432.
Michelin JLH. 1840–1847. Iconographie zoophytologique, description par localités et terrains des Polypiers fossiles de la France et pays environnants. Vol. 2 P. Bertrand: Paris. pp 1–348.
Milne Edwards H, Haime J. 1849. Observations sur les polypiers de la famille des astréides. C R Acad Sci 29:465–470.
Moseley HN. 1876. Preliminary report to professor Wyville Thomson, F.R.S., director of the civilian scientific staff, on the true corals dredged by H.M.S. "Challenger" in deep water between the dates Dec. 30th, 1870, and August 31st, 1875. P. R. Soc. London 24:544–569.
Moseley HN. 1881. Report on certain hydroid, alcyonarian and madreporarian corals procured during the Voyage of H.M.S. Challenger, in the years 1873–1876. Report on the Scientific Results of the Voyage of H.M.S. Challenger. Zoology 2:1–101,209–230.
Nothdurft LD, Webb G. 2007. Microstructure of common reef-building coral genera *Acropora*, *Pocillopora*, *Goniastrea* and *Porites*: Constraints on spatial resolution in geochemical sampling. Facies 53:1–26.
Ogilvie MM. 1897. Die Korallen der Strambergerschichten. Palaeontogr Supp 2:73–282.
Owens JM. 1984. Microstructural changes in the *Micrabaciidae* and their ecologic and taxonomic implications. Palaeontogr Am 54:519–522.
Owens JM. 1986. *Rhombopsammia*, a new genus of the family Micrabaciidae. Proc Biol Soc Wash 99:248–256.
Puverel S, Tambutte E, Zoccola D, Domart-Coulon I, Bouchot A, Lotto S, Allemand D, Tambutte S. 2005. Antibodies against the organic matrix in scleractinians: A new tool to study coral biomineralization. Coral Reefs 24:149–156.
Przeniosło R, Stolarski J, Mazur M, Brunelli M. 2008. Hierarchically structured scleractinian coral biocrystals. J Struct Biol 161:74–82.
Reyes-Bermudez A, Lin Z, Hayward DC, Miller DJ, Ball EE. 2009. Differential expression of three galaxin-related genes during settlement and metamorphosis in the scleractinian coral *Acropora millepora*. BMC Evol Biol 9:178; doi:10.1186/1471–2148-9–178.
Schöne BR, Dunca E, Fiebig J, Pfeiffer M. 2005. Mutvei's solution: An ideal agent for resolving microgrowth structures of biogenic carbonates. Palaeogeogr Palaeoclimatol Palaeoecol 228:149–166.
Stolarski J. 2000. Origin and phylogeny of Guyniidae (Scleractinia) in the light of microstructural data. Lethaia 33:13–38.
Stolarski J. 2003. Three-dimensional micro- and nanostructural characteristics of the scleractinian coral skeleton: A biocalcification proxy. Acta Palaeontol Pol 48:497–530.
Stolarski J. 2007. "Weaving" of the fibrous skeleton of Scleractinia. 10th International Symposium of Fossil Cnidaria and Porifera, St. Petersburg, 2007, August 12–16 (Abstracts), 89.
Stolarski J, Mazur M. 2005. Nanostructure of biogenic versus abiogenic calcium carbonate crystals. Acta Palaeontol Pol 50:847–865.
Stolarski J, Roniewicz E. 2001. Towards a new synthesis of evolutionary relationships and classification of Scleractinia. J Paleontol 75:1090–1108.
Vaughan TW, Wells JW. 1943. Revision of the suborders, families, and genera of the Scleractinia. Geol Soc Spec Paper 104:1–363.
Wallace CC, Wolstenholme J. 1998. Revision of the coral genus *Acropora* (Scleractinia: Astrocoeniina: Acroporidae) in Indonesia. Zool J Linn Soc 123:199–384.
Wei NV, Wallace CC, Dai C-F, Pillay KRM, Chen CA. 2006. Analyses of the ribosomal internal transcribed spacers (ITS) and the 5.8S gene indicate that extremely high rDNA heterogeneity is a unique feature in the scleractinian coral genus *Acropora* (Scleractinia; Acroporidae). Zool Stud 45:404–418.
Wells JW. 1933. Corals of the cretaceous of the Atlantic and Gulf plains and Western interior of the United States. Bull Am Paleontol 18:85–288.
Wise SW. 1972. Observations of fasciculi on developmental surfaces of scleractinian coral exoskeletons. Biomineral Res Rep 6:160–175.
Wise SW, Stieglitz RD, Hay WW. 1970. Scanning electron microscope study of fine grain size biogenic carbonate particles. Gulf Coast Assoc Geol SocTrans 20:287–302.
Yabe H, Eguchi M. 1932. Some recent and fossil corals of the genus *Stephanophyllia* H. Michelin from Japan. Sci Rep Tohoku Univ, Ser 2 (Geology) 15:55–63.